Refined Glauber model versus Faddeev calculations and experimental data for *pd* spin observables

M. N. Platonova* and V. I. Kukulin†

D.V. Skobeltsyn Institute of Nuclear Physics, M.V. Lomonosov Moscow State University, Moscow RU-119991, Russia

(Received 5 November 2009; published 15 January 2010)

Spin-dependent observables in intermediate-energy *pd* elastic scattering within the framework of the refined Glauber model are considered. The improvements include an account of all ten *pp* and *pn* helicity amplitudes at respective energies constructed on the basis of modern phase-shift analysis, accurate deuteron wave functions taken from the modern *NN* force model and account of charge-exchange effects. Predictions of the refined diffraction model for differential cross section and analyzing powers are compared with exact three-body Faddeev calculations and the recent experimental data. An amazingly good agreement between the results of both theoretical approaches as well as between the refined Glauber model and experiment in a wide angular range not only for differential cross section but also for vector and tensor analyzing powers has been found for the first time. Possible reasons for this agreement are discussed.

DOI: 10.1103/PhysRevC.81.014004 PACS number(s): 21.45.−v, 24.10.Ht, 24.70.+s, 25.40.Cm

I. INTRODUCTION

It is well known that the Glauber diffraction model [1,2] is a convenient and reliable tool for the analysis of scattering of fast nucleons (and other hadrons) by nuclei. Based on the eikonal and fixed-scatterer approximations, it was specially developed more than 50 years ago for the high- and intermediate-energy regions where no exact theoretical treatments were available. So, the validity of the Glauber model could be tested previously only by comparing its results with the respective experimental data. The unexpected success of such a simple model in describing the hadron-nucleus and nucleus-nucleus scattering at forward angles induced numerous studies of the accuracy and the range of validity of the Glauber formulation, as well as many attempts to extend this range. Different refinements of the initial simple model have been introduced since then, and they included corrections for non-eikonal and relativistic effects, Fermi motion, etc. The last (in time) substantial steps taken in this direction can be found in Refs. [3–6]. However, the comprehensive analysis of various corrections to the Glauber model has revealed [7] that many important corrections tend to compensate strongly each other, so that an incorporation of only one of them can even worsen the results of the original simple model. So, it turned out to be highly nontrivial to improve the initial Glauber approach.

Another serious problem with this model seems its rather restricted range of applicability, i.e., it should work well, in general, at sufficiently high energies and forward angles. However, it would be extremely interesting (for many practical applications) to know these limits more definitely, although they are dependent upon the particular problem to be solved. Fortunately, nowadays we can learn much more than before about these limits for some important cases by comparing the predictions of the Glauber model against the results of precise calculations within the framework of the respective fundamental approaches, i.e., without approximations peculiar to the diffraction model. Among these cases allowing the careful comparison with a numerically accurate treatment is the *Nd* intermediate-energy scattering within a realistic three-body model. Now we have a very nice opportunity to examine the accuracy of the Glauber model by direct comparison of its predictions with exact three-nucleon Faddeev calculations [8] which account for the same (nucleonic) degrees of freedom and the same input on-shell *NN* amplitudes. Such a test will show qualitatively or even quantitatively the validity of different approximations involved in the Glauber formulation. To obtain fully realistic conclusions, the Glauber model itself must be as realistic as possible; i.e., it should include all fully realistic input spin-dependent *NN* amplitudes and all components of the target (e.g., deuteron) wave function. Such generalization of the initial model enables us to analyze the spin observables (which should be much more sensitive to fine interference effects and different approximations) as well as the unpolarized cross sections, so we will be able to draw more quantitative and well-grounded conclusions about the validity of the Glauber approach. For a meaningful comparison with exact three-body calculations, the inputs of the model, i.e., *NN* amplitudes and deuteron wave functions, must also be the most accurate and coincide with those used in the current Faddeev calculations. Because the diffraction model includes on-shell *NN* amplitudes only, they can be taken from the experiment. Or, more definitely, one can derive these amplitudes from modern phase-shift analysis (PSA), so that they will be on-shell equivalent to those found with realistic *NN* potentials entering the Faddeev equations (in, of course, the energy region where such potentials describe accurately the *NN* experimental data).

The fully realistic Faddeev equations for *Nd* scattering have been solved up to now only for the incident energies $T_N \leqslant 250$ MeV in the laboratory frame [9,10].[1] Complications which arise with growing energy are connected with limitations of highly precise *NN* potentials involved as well as with

*platonova@nucl-th.sinp.msu.ru
†kukulin@nucl-th.sinp.msu.ru

[1]There is only a single full three-body calculation [11] for *pd* scattering at the proton incident energy $T_p \simeq 400$ MeV, but its results are still preliminary and have not been published yet.

hard computational problems. Recently [12], the Faddeev calculations at higher energies (up to 2 GeV) have been carried out, but only in a schematic model with three identical bosons interacting through a scalar central potential of the Malfliet-Tjon type. In this model, a detailed comparison with the Glauber approach for total and differential elastic cross sections was also performed [13].

In the present paper, we tested the validity of the Glauber model with a fully realistic two-body input. First, we generalized the initial model by incorporating the full spin dependence of the *NN* amplitudes and deuteron wave function as well as the charge-exchange effects. We analyzed the differential cross sections and polarization observables for *pd* elastic scattering in the energy region of a few hundred MeV, which seems already high enough to apply the generalized Glauber approach but still low enough to compare its predictions with those of exact realistic Faddeev calculations. Moreover, it was demonstrated [9] that at such moderate energies, relativistic effects do not play a significant role at small and medium scattering angles, so the nonrelativistic treatment seems to be sufficient on such conditions. To confirm our conclusions and to obtain a more clear understanding of the phenomena in question, the comparison of the results for both theoretical approaches, i.e., Glauber and Faddeev, with available experimental data is also presented. From all these comparisons, one can draw more definite conclusions about the true range of validity of the refined Glauber model presented here.

The content of the paper is as follows. In Sec. II, we generalize the initial diffraction model by incorporating all ten *NN* helicity amplitudes (five are for *pp* and five are for *pn* scattering) and develop a convenient Gaussian-like parametrization of these amplitudes. Also we build a multi-Gaussian expansion for realistic deuteron *S*- and *D*-wave functions. The convenient analytical representation for main input ingredients of the model makes it possible to derive all 12 invariant *pd* amplitudes in fully analytical forms. In Sec. III, we present the main results of the work. The detailed and comprehensive discussion of the obtained results and some physical arguments which can help to interpret our findings more clearly are presented in Sec. IV. Our concluding remarks are given in Sec. V. Two appendixes include some important details of the calculations within the framework of the refined Glauber model. In Appendix A, we present the explicit interrelations between all *pd* and *NN* invariant amplitudes. In Appendix B, the details of analytical integration in the double-scattering amplitudes are given.

II. REFINED GLAUBER MODEL

To explore high-precision spin-dependent *NN* interactions for describing *pd* elastic scattering, the conventional Glauber model and its basic formulas which relate *pd* amplitude to the input *NN* amplitudes and the deuteron wave function have to be generalized. In preceding years, some papers have been published that considered the following contributions separately: (i) spin dependence of *NN* amplitudes [14,15], (ii) *D* wave of the deuteron [16,17], and (iii) isospin dependence of *NN* amplitudes, i.e., double charge-exchange contribution to *pd* elastic scattering [18,19]. All these items were included later in the so-called relativistic multiple-scattering theory [5,6] which went beyond the Glauber framework by accounting for corrections to the eikonal and fixed-scatterer approximations and some relativistic effects as well. It is well known, at least qualitatively, that different corrections to the Glauber model tend to cancel each other substantially [7], so it is hard to improve essentially the Glauber model. Besides, the modified versions are much more complicated than the initial model. So, we have generalized just the initial Glauber formulation by including the above-mentioned items without any further corrections to the diffraction model itself, thus staying within the original Glauber framework.

A. Definition of observables

First of all, we need to define the differential cross section and spin-dependent observables in terms of the *pd* elastic-scattering amplitude. The differential cross section is connected to the above amplitude M by the relation[2]

$$d\sigma/dt = \tfrac{1}{6}\mathrm{Sp}(MM^{+}), \tag{1}$$

where $t = -q^2$ is the momentum transfer squared.[3] As for spin-dependent observables, in this work we concentrate mainly on the vector and tensor analyzing powers. For the proton and deuteron vector analyzing powers (A_α^p and A_α^d) and for the deuteron tensor analyzing powers ($A_{\alpha\beta}$) we take the standard formulas

$$\begin{aligned} A_\alpha^p &= \mathrm{Sp}(M\sigma_\alpha M^{+})/\mathrm{Sp}(MM^{+}),\\ A_\alpha^d &= \mathrm{Sp}(MS_\alpha M^{+})/\mathrm{Sp}(MM^{+}),\\ A_{\alpha\beta} &= \mathrm{Sp}(MS_{\alpha\beta} M^{+})/\mathrm{Sp}(MM^{+}), \end{aligned} \tag{2}$$

where $\frac{1}{2}\sigma_\alpha$ and $S_\alpha = \frac{1}{2}(\sigma_{n\alpha} + \sigma_{p\alpha})$ are the spin matrices of the proton and deuteron, $S_{\alpha\beta} = \frac{3}{2}(S_\alpha S_\beta + S_\beta S_\alpha) - 2\delta_{\alpha\beta}$ is a quadrupole operator, and $\alpha, \beta \in \{x, y, z\}$.

The total amplitude M can be expanded on the amplitudes invariant under space rotations and space-time reflections. For the *pd* case, there are 12 such invariant amplitudes A_1–A_{12}, and the amplitude M (in nonrelativistic formulation) is expressed

[2]Our normalization is different from the standard one by the Lorentz-invariant factor $8\sqrt{\pi}I(s, m_p, m_d) \equiv 4\sqrt{\pi[s-(m_p+m_d)^2][s-(m_p-m_d)^2]}$, where s is the *pd* invariant mass squared, and m_p and m_d are the proton and deuteron masses. Such normalization is chosen in order to simplify the final formulas.

[3]Although we work in the laboratory frame according to the initial Glauber suggestion, we should throughout keep in mind the relation $t = -q^2$ for consistency. This relation is valid in the center-of-mass frame and approximately valid in the laboratory frame at small momentum transfers. Physically, the difference between the variables t in these two frames originates from recoil effects which are neglected in the Glauber formalism due to the fixed-scatterer approximation. So, this difference should not be accounted for without careful treatment of recoil effects as well as other corrections to the Glauber model which all become significant at large momentum transfers.

through them as

$$M[\mathbf{p},\mathbf{q};\boldsymbol{\sigma},\mathbf{S}] = (A_1 + A_2\boldsymbol{\sigma}\hat{n}) + (A_3 + A_4\boldsymbol{\sigma}\hat{n})(\mathbf{S}\hat{q})^2 + (A_5 + A_6\boldsymbol{\sigma}\hat{n})(\mathbf{S}\hat{n})^2 + A_7(\boldsymbol{\sigma}\hat{k})(\mathbf{S}\hat{k}) + A_8\boldsymbol{\sigma}\hat{q}((\mathbf{S}\hat{q})(\mathbf{S}\hat{n})+(\mathbf{S}\hat{n})(\mathbf{S}\hat{q})) + (A_9 + A_{10}\boldsymbol{\sigma}\hat{n})\mathbf{S}\hat{n} + A_{11}(\boldsymbol{\sigma}\hat{q})(\mathbf{S}\hat{q}) + A_{12}\boldsymbol{\sigma}\hat{k}((\mathbf{S}\hat{k})(\mathbf{S}\hat{n})+(\mathbf{S}\hat{n})(\mathbf{S}\hat{k})), \quad (3)$$

where the unit vectors $\hat{k} = (\mathbf{p}+\mathbf{p}')/|\mathbf{p}+\mathbf{p}'|$, $\hat{q} = (\mathbf{p}-\mathbf{p}')/|\mathbf{p}-\mathbf{p}'|$, and $\hat{n} = \hat{k}\times\hat{q}$; and $\mathbf{p}$ and $\mathbf{p}'$ are the momenta of the incident and outgoing proton, respectively.

Now all the *pd* observables can be written in terms of the invariant amplitudes A_1–A_{12}. Defining the directions of coordinate axes $\hat{e}_x = \hat{q}$, $\hat{e}_y = \hat{n}$, and $\hat{e}_z = \hat{k}$, and applying the standard trace technique, one gets for the differential cross section and nonvanishing analyzing powers the following expressions:

$$\begin{aligned}
d\sigma/dt &= |A_1|^2 + |A_2|^2 + \frac{2}{3}\left(\sum_{i=3}^{12}|A_i|^2 + \mathrm{Re}[2A_1^*(A_3+A_5) + 2A_2^*(A_4+A_6) + A_3^*A_5 + A_4^*A_6]\right),\\
A_y^p &= 2\mathrm{Re}[2(A_1^*+A_3^*+A_5^*)(A_2+A_4+A_6) + A_1^*A_2 - A_3^*A_6 - A_4^*A_5 + 2A_9^*A_{10}]/(3d\sigma/dt),\\
A_y^d &= 2\mathrm{Re}[(2A_1^*+A_3^*+2A_5^*)A_9 + (2A_2^*+A_4^*+2A_6^*)A_{10} + A_7^*A_{12} + A_8^*A_{11}]/(3d\sigma/dt),\\
A_{yy} &= (2(|A_5|^2+|A_6|^2+|A_9|^2+|A_{10}|^2) - (|A_3|^2+|A_4|^2 + |A_7|^2+|A_8|^2+|A_{11}|^2+|A_{12}|^2) + 2\mathrm{Re}[A_1^*(2A_5-A_3) + A_2^*(2A_6-A_4) + A_3^*A_5 + A_4^*A_6])/(3d\sigma/dt),\\
A_{xx} &= (2(|A_3|^2+|A_4|^2+|A_{11}|^2+|A_{12}|^2) - (|A_5|^2+|A_6|^2+|A_7|^2+|A_8|^2+|A_9|^2+|A_{10}|^2) + 2\mathrm{Re}[A_1^*(2A_3-A_5) + A_2^*(2A_4-A_6) + A_3^*A_5 + A_4^*A_6])/(3d\sigma/dt),\\
A_{zz} &= -A_{yy} - A_{xx},\\
A_{xz} &= \mathrm{Im}[A_3^*A_9 + A_4^*A_{10} - A_7^*A_{12} - A_8^*A_{11}]/(d\sigma/dt).
\end{aligned} \quad (4)$$

B. Generalization of initial Glauber formalism

In the initial Glauber model, the *pd* scattering amplitude as the function of transferred momentum $\mathbf{q}$ is represented as a sum of two terms corresponding to single and double scatterings of the incident proton by the target nucleons:

$$M(\mathbf{q}) = M^{(s)}(\mathbf{q}) + M^{(d)}(\mathbf{q}). \quad (5)$$

With the use of eikonal and fixed-scatterer approximations, the single- and double-scattering amplitudes are expressed in terms of the on-shell *NN* amplitudes (*pp* amplitude M_p and *pn* amplitude M_n) and the deuteron wave function Ψ_d as

$$\begin{aligned}
M^{(s)}(\mathbf{q}) &= \int d^3r e^{i\mathbf{qr}/2}\Psi_d(\mathbf{r})[M_n(\mathbf{q}) + M_p(\mathbf{q})]\Psi_d(\mathbf{r}),\\
M^{(d)}(\mathbf{q}) &= -\frac{i}{4\pi^{3/2}}\int d^2q'\int d^3r e^{i\mathbf{q}'\mathbf{r}}\Psi_d(\mathbf{r})[M_n(\mathbf{q_2})M_p(\mathbf{q_1}) + M_p(\mathbf{q_1})M_n(\mathbf{q_2})]\Psi_d(\mathbf{r}),
\end{aligned} \quad (6)$$

where the vectors $\mathbf{q_1} = \mathbf{q}/2 - \mathbf{q}'$ and $\mathbf{q_2} = \mathbf{q}/2 + \mathbf{q}'$ have been introduced for momenta transferred in collisions with individual target nucleons.[4]

The double-charge-exchange process contributes to elastic scattering as well. This contribution is significant at incident energies $T_p \lesssim 1$ GeV, so we should include it in the model. It was already done in Ref. [19] by incorporating the isospin structure of the general *NN* amplitude and averaging over the isoscalar deuteron ground state. This operation leads to an additional term in the double-scattering amplitude

$$M^{(c)}(\mathbf{q}) = \frac{i}{4\pi^{3/2}}\int d^2q'\int d^3r e^{i\mathbf{q}'\mathbf{r}}\Psi_d(\mathbf{r})[M_n(\mathbf{q_2}) - M_p(\mathbf{q_2})][M_n(\mathbf{q_1}) - M_p(\mathbf{q_1})]\Psi_d(\mathbf{r}). \quad (7)$$

The neglect of spin dependence in *NN* amplitudes and deuteron wave function reduces Eqs. (5) and (6) to the conventional Glauber formulas. Furthermore, the double-charge-exchange amplitude $M^{(c)}$ vanishes in a widely used approximation $M_n = M_p$ (it corresponds to the neglect of isospin dependence in the general *NN* amplitude). In the realistic case, with which we are here concerned, the accurate incorporation of both spin and isospin degrees of freedom is required. While the latter is done simply by adding the term $M^{(c)}$ to the double-scattering amplitude $M^{(d)}$, the account for the full spin structure of *NN* amplitudes and deuteron wave function in the Glauber model is much more involved. We take the *NN* amplitudes in the form

$$M_i[\mathbf{p},\mathbf{q};\boldsymbol{\sigma},\boldsymbol{\sigma}_i] = A_i + C_i\boldsymbol{\sigma}\hat{n} + C_i'\boldsymbol{\sigma}_i\hat{n} + B_i(\boldsymbol{\sigma}\hat{k})(\boldsymbol{\sigma}_i\hat{k}) + (G_i+H_i)(\boldsymbol{\sigma}\hat{q})(\boldsymbol{\sigma}_i\hat{q}) + (G_i-H_i)(\boldsymbol{\sigma}\hat{n})(\boldsymbol{\sigma}_i\hat{n}), \quad (8)$$

where $i = n, p$. In the laboratory frame, one should distinguish the amplitudes C and C'.

For the deuteron wave function, we use the standard expression

$$\Psi_d[\mathbf{r};\boldsymbol{\sigma}_n,\boldsymbol{\sigma}_p] = \frac{1}{\sqrt{4\pi}r}\left(u(r) + \frac{1}{2\sqrt{2}}w(r)S_{12}[\hat{r};\boldsymbol{\sigma}_n,\boldsymbol{\sigma}_p]\right), \quad (9)$$

where u and w are the radial wave functions for S and D waves, and $S_{12}[\hat{n};\mathbf{v}_1,\mathbf{v}_2] = 3(\mathbf{v}_1\hat{n})(\mathbf{v}_2\hat{n}) - (\mathbf{v}_1\mathbf{v}_2)$.

After substituting expressions (8) and (9) into Eqs. (6) and (7) and making some spin algebra with noncommuting operators M_n, M_p, and Ψ_d, one gets rather complicated general

[4] In the expression (6) for the amplitude $M^{(d)}(\mathbf{q})$, we have omitted the term arising from the commutator of the amplitudes $M_n(\mathbf{q_2})$ and $M_p(\mathbf{q_1})$ [19]. This term gives only a small contribution to the intermediate-energy *pd* elastic scattering due to the relative smallness of the spin-dependent *NN* amplitudes and the deuteron *D* wave.

formulas for the pd amplitudes $M^{(s)}$, $M^{(d)}$, and $M^{(c)}$ expressed through the input NN amplitudes $A_i, B_i, C_i, C_i', G_i, H_i$ $(i = n, p)$ and deuteron wave functions u, w. To simplify further derivation, one can employ the smallness of the spin-dependent NN amplitudes (say, $\mathcal{B}_i$) compared to spin-independent ones (A_i) at high energies as well as the smallness of the deuteron D wave w compared to S wave u [20]. So, the terms containing products $\mathcal{B}_i^k w^l$ with $k + l \geqslant 3$ can be dropped out of the expressions for the amplitudes $M^{(s)}$, $M^{(d)}$, and $M^{(c)}$ on definite conditions. In fact, the ratio of spin-dependent $\mathcal{B}_i$ to spin-independent amplitudes A_i is strongly decreasing when the energy rises, so that such an approximation in the pd amplitudes, being quite accurate at intermediate energies $T_p \sim 1$ GeV, can be unsatisfied at lower energies $T_p \sim 100$ MeV. This observation has nothing to do with the validity of the Glauber model itself at such lower energies, and it should be kept in mind when doing the careful comparison between the present version of the Glauber model and experimental data for spin analyzing powers (especially for tensor ones, which are more sensitive to fine spin-dependent effects) in Sec. III.

After the above simplification, Eqs. (6) and (7) can be easily integrated over d^3r. In doing this, we make use of the deuteron form factor, which is defined as

$$S[\mathbf{q}; \boldsymbol{\sigma}_n, \boldsymbol{\sigma}_p] = \int d^3r e^{i\mathbf{qr}} |\Psi_d[\mathbf{r}; \boldsymbol{\sigma}_n, \boldsymbol{\sigma}_p]|^2 = S_0(q) - \frac{1}{2\sqrt{2}} S_2(q) S_{12}[\hat{q}; \boldsymbol{\sigma}_n, \boldsymbol{\sigma}_p]. \quad (10)$$

It is convenient to divide the monopole and quadrupole form factors, S_0 and S_2, into two parts which correspond to different multiplicities of the D-wave function w, i.e.,

$$S_0(q) = S_0^{(0)}(q) + S_0^{(2)}(q), \quad S_2(q) = S_2^{(1)}(q) + S_2^{(2)}(q), \quad (11)$$

where

$$\begin{aligned} S_0^{(0)}(q) &= \int_0^\infty dr u^2(r) j_0(qr), \\ S_0^{(2)}(q) &= \int_0^\infty dr w^2(r) j_0(qr), \\ S_2^{(1)}(q) &= 2\int_0^\infty dr u(r) w(r) j_2(qr), \\ S_2^{(2)}(q) &= -2^{-1/2} \int_0^\infty dr w^2(r) j_2(qr). \end{aligned} \quad (12)$$

Eventually, using the expansion (3) for the total pd amplitude M, one obtains the explicit interrelations between all 12 invariant pd amplitudes and 12 invariant input NN amplitudes and also different components of the deuteron form factor (for the final formulas and details of analytic $\mathbf{q}'$ integration in the double-scattering amplitudes, see Appendixes A and B, respectively). Having these interrelations and proper two-body input in hand, one can calculate straightforwardly the pd differential cross section and all polarization observables on the basis of the refined Glauber model.

C. Parametrization of the NN amplitudes and deuteron wave function

The Glauber model deals with pd and NN amplitudes defined in the laboratory frame. However, it is more convenient to treat the NN helicity amplitudes in the two-nucleon center-of-mass frame. It is easy to show that the laboratory amplitudes A, B, C, G, H at small values of q can be straightforwardly expressed through the conventional helicity amplitudes N_0, N_1, N_2, U_0, U_2 (or ϕ_1–ϕ_5) as

$$\begin{aligned} A &\approx N_0 = (\phi_3 + \phi_1)/2, \\ B &\approx -U_0 = (\phi_3 - \phi_1)/2, \\ C &\approx iN_1 = i\phi_5, \\ G &\approx (U_2 - N_2)/2 = \phi_2/2, \\ H &\approx (U_2 + N_2)/2 = \phi_4/2. \end{aligned} \quad (13)$$

Here, in making appropriate approximations, we do not go beyond the diffraction model. It was also demonstrated [21] that the amplitude C' [see Eq. (8)] in the high-energy small-angle limit is distinguished only by a relativistic correction from the amplitude C, i.e.,

$$C' \approx C + (q/2m)N_0. \quad (14)$$

Moreover, both the amplitudes C and C' are small at high energies compared to the other amplitudes, so the above correction hardly plays a significant role, but it still should be included for consistency.

All the helicity pp and pn amplitudes at the energy $T_p = 1$ GeV are displayed in Fig. 1. These amplitudes are built in the present work on the basis of recent PSA [22], and we used a special code [23] to reconstruct the pp and pn helicity amplitudes from the PSA data. As clearly seen from Fig. 1, the amplitude N_0 is significantly superior to all the other helicity amplitudes. It is also clearly seen that the corresponding pp and pn amplitudes are distinguished from each other significantly, whereas in early studies of the diffraction model, they were often chosen to be the same for the sake of simplicity.

To parametrize the NN helicity amplitudes, it is very convenient to employ a Gaussian series representation with an explicit separation of the behavior near $q = 0$:

$$\begin{aligned} N_0(q) &= \sum_{j=1}^n C_{a,j} \exp(-A_{a,j} q^2), \\ U_0(q) &= \sum_{j=1}^n C_{b,j} \exp(-A_{b,j} q^2), \\ N_1(q) &= q \sum_{j=1}^n C_{c,j} \exp(-A_{c,j} q^2), \\ [U_2(q) - N_2(q)]/2 &= \sum_{j=1}^n C_{g,j} \exp(-A_{g,j} q^2), \\ [U_2(q) + N_2(q)]/2 &= q^2 \sum_{j=1}^n C_{h,j} \exp(-A_{h,j} q^2). \end{aligned} \quad (15)$$

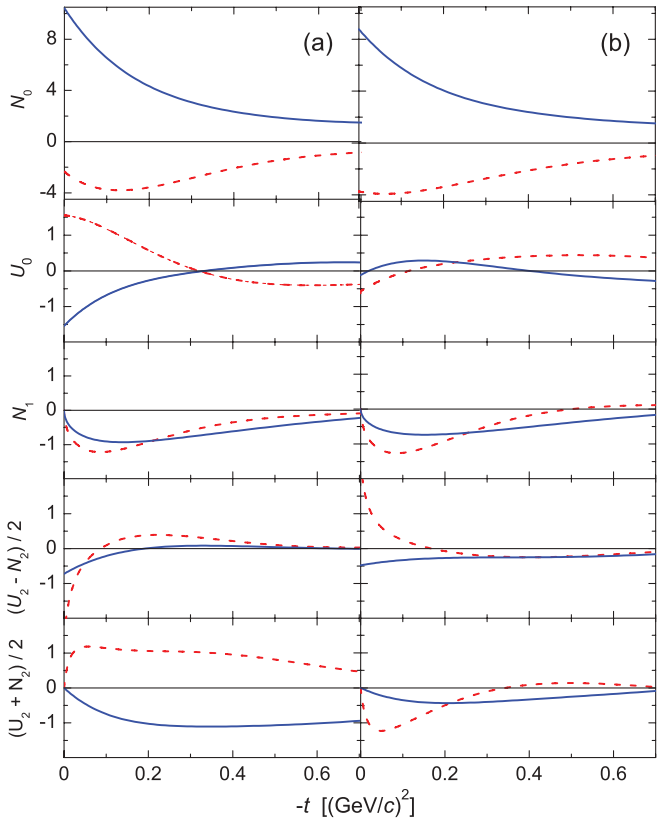

FIG. 1. (Color online) Combinations of the *NN* helicity amplitudes (in units $\sqrt{\text{mb}}$/GeV), which correspond to the laboratory *NN* amplitudes used in our calculations [see Eq. (13)]. The *pp* amplitudes are shown in column (a), the *pn* amplitudes are given in column (b). The dashed lines correspond to the real parts of the amplitudes, while the solid lines represent their imaginary parts.

Here the subscripts a, b, c, g, h in the parameters C, A denote the respective laboratory *NN* amplitudes [see Eq. (13)].[5] In our calculations, we took $n = 5$, i.e., five Gaussian terms in all the above sums. With this choice, we found that the Gaussian approximated *NN* amplitudes are very near to the exact ones in the forward hemisphere [20]. The visible deviations begin only at large angles, where the Glauber model demands a fast vanishing of all the underlying amplitudes. The rise in magnitude of the true *pp* helicity amplitudes is due to the Pauli principle, according to which the whole *pp* amplitude must be antisymmetrized. This antisymmetrization is essential in large-angle *pd* scattering only through a one-nucleon exchange mechanism, so the diffraction model being derived for forward-angle scattering does not account for this exchange mechanism. On the other hand, the charge-exchange process which is responsible for the rising of *np* helicity amplitudes at large angles can contribute to *pd* elastic scattering already at rather forward angles through the double charge exchange, and thus, the latter mechanism is included in our formalism explicitly.

For the deuteron wave function, we explored the high-precision *NN* potential model CD-Bonn [24]. To parametrize *S*- and *D*-wave components of the function, we also employed the Gaussian representation (with an additional factor r^n to reproduce the behavior near the origin):

$$u(r) = r\sum_{j=1}^{m} C0_j \exp(-A0_j r^2),$$
$$w(r) = r^3\sum_{j=1}^{m} C2_j \exp(-A2_j r^2). \tag{16}$$

In our calculations, we have chosen $m = 5$. With this number of terms, the approximated deuteron wave functions coincide with high accuracy with the exact ones from the origin up to large distances ($r_{NN} \simeq 20$ fm). With the above parametrization of the deuteron radial wave functions, the form factors defined in Eq. (12) take the forms

$$S_0^{(0)}(q) = \sum_{i,j=1}^{m} C0_i C0_j \frac{\sqrt{\pi}}{4\lambda_{00,ij}^{3/2}} \exp(-x_{00,ij}),$$
$$S_0^{(2)}(q) = \sum_{i,j=1}^{m} C2_i C2_j \frac{\sqrt{\pi}}{16\lambda_{22,ij}^{7/2}} \left(4x_{22,ij}^2 - 20x_{22,ij} + 15\right) \times \exp(-x_{22,ij}),$$
$$S_2^{(1)}(q) = \sum_{i,j=1}^{m} C0_i C2_j \frac{\sqrt{\pi}}{2\lambda_{02,ij}^{5/2}} x_{02,ij} \exp(-x_{02,ij}),$$
$$S_2^{(2)}(q) = \sum_{i,j=1}^{m} C2_i C2_j \frac{\sqrt{2\pi}}{16\lambda_{22,ij}^{7/2}} \left(2x_{22,ij}^2 - 7x_{22,ij}\right) \exp(-x_{22,ij}), \tag{17}$$

where $\lambda_{kl,ij} = Ak_i + Al_j$, $x_{kl,ij} = q^2/(4\lambda_{kl,ij})$, and $k, l = 0, 2$.

III. RESULTS

Using the above refined Glauber model, we analyzed the *pd* differential cross sections as well as proton and deuteron analyzing powers at three intermediate energies: $T_p = 250$ and 440 MeV and 1 GeV.[6] These energies were chosen because there is a considerable amount of experimental data on *pd* elastic observables in these energy regions [11,25–30]. Besides that, the two lower energies are appropriate for comparing in detail the predictions of our model with exact Faddeev results.

We start with the energy $T_p = 250$ MeV because the realistic Faddeev calculations are well grounded for this energy. Results for *pd* differential cross section and proton

[5] In explicit calculations, we explored two different relations (and two sets of parameters C, A) for each helicity amplitude, i.e., one for its real part and one for the imaginary part. So all parameters really need two additional indices, say, $i = n, p$ (to distinguish *pp* and *np* amplitudes) and $k = r, i$ (to distinguish real and imaginary parts). Here, just the general forms that fit both real and imaginary parts of *pp* as well as *pn* amplitudes are given for transparency.

[6] For the deuteron analyzing powers which are measured in *dp* scattering, these are the equivalent proton incident energies in the inverse kinematics, i.e., $T_p = T_d/2$.

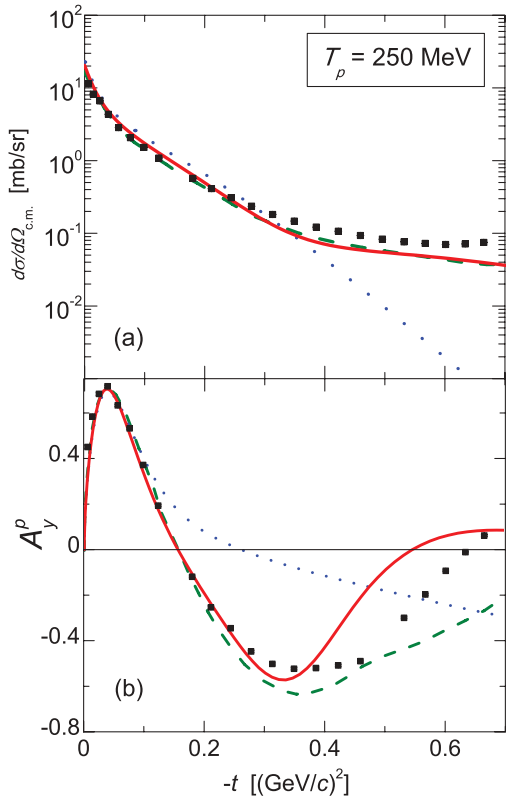

FIG. 2. (Color online) Differential cross section (a) and proton analyzing power (b) in *pd* elastic scattering at the incident energy $T_p = 250$ MeV. The solid lines represent the results obtained within the refined Glauber model, the dotted lines show the single-scattering contribution only, while the dashed lines correspond to predictions of the exact Faddeev calculations [25] with *NN* potential CD-Bonn. Experimental data (squares) are taken from Ref. [25].

analyzing power at $T_p = 250$ MeV are represented in Fig. 2. We also calculated the deuteron vector and tensor analyzing powers at the equivalent proton energy $T_p = 250$ MeV. However, the exact Faddeev results and experimental data for these observables are available in the literature just for a bit lower energy, $T_p = 200$ MeV. Our separate comparison between some experimental data at $T_p = 200$ and 250 MeV has shown that they are very close to each other. So, our predictions for the deuteron vector and tensor analyzing powers at $T_p = 250$ MeV in comparison with exact three-body results and experimental data at $T_p = 200$ MeV are displayed in Fig. 3. In addition, we show the results of the refined Glauber model at $T_p = 440$ MeV (see Fig. 4). The Faddeev calculations with the fully realistic *NN* interaction are not so reliable for this energy; thus, we restrict ourselves with the differential cross section and the proton analyzing power. We compared our result for differential cross section at the energy $T_p = 440$ MeV with the Faddeev calculation at the same energy and with experimental data at $T_p = 425$ MeV. For the comparison with our result for proton analyzing power at $T_p = 440$ MeV, we employed existing (to date) Faddeev calculation and experimental data at a bit lower energy, $T_p = 392$ MeV.

Besides the comparison between the refined Glauber model predictions and exact three-body Faddeev results, it would be highly interesting to compare our results with existing experimental data at the higher energy of $T_p = 1$ GeV, which is more traditional for the diffraction model. This comparison has been made for the differential cross section as well as for deuteron vector and tensor analyzing powers. In Fig. 5, the predictions of our model together with respective experimental data are displayed.

It is clearly seen from Figs. 2–5 that our results found within the refined Glauber model are, in general, in very reasonable agreement with both exact three-body calculations and experimental data at transferred momenta squared $|t| \lesssim 0.3$–0.4 (GeV/c)^2 for differential cross sections and vector and tensor analyzing powers as well.[7] This gives, at first glance, some interesting deep puzzle because the good agreement with the exact Faddeev calculations is seen in the region where the double scattering (in the Glauber model) dominates. However, instead of two purely on-shell and no-recoil scatterings of the incident proton by two nucleons in deuteron within the Glauber model framework, the Faddeev calculations include many fully off-shell rescatterings with full account of recoil effects. We will discuss in detail some possible physical reasons for such an amazing agreement in the next section.

Moreover, on Figs. 2–4, one can see a general new trend: in those kinematical regions (at larger $|t|$) where the refined diffraction model deviates essentially from the exact Faddeev theory, the exact $3N$ results begin also to deviate from the experimental data. This gives another interesting question to answer.

IV. DISCUSSION

It would be useful to arrange the general discussion of the results obtained in this paper in a few separate points.

(i) Fully analytical formulas which relate all 12 invariant *pd* amplitudes to the accurate input *pp* and *pn* helicity amplitudes (see Appendixes A and B) allow us to not only greatly simplify all the numerical calculations for *pd* spin observables but also to develop an efficient and convenient algorithm for solving an important *inverse scattering problem* (at fixed energy). This inverse problem can be formulated as follows:

(a) Having the precise intermediate-energy *nd* spin observables and differential cross section and by taking the respective *np* helicity amplitudes at the same energy as a well-established input, one can extract poorly known neutron-neutron scattering amplitudes at the same energy.

[7] The agreement for tensor analyzing powers at rather low energies ($T_p \simeq 250$ MeV) is not as good as that for differential cross sections and vector analyzing powers (see Figs. 2 and 3). This fact is very likely related to our simplifying assumption about the relative smallness of the spin-dependent *NN* amplitudes in comparison to the large spin-independent ones (see the end of Sec. II B) and not to the validity of the Glauber approximation itself.

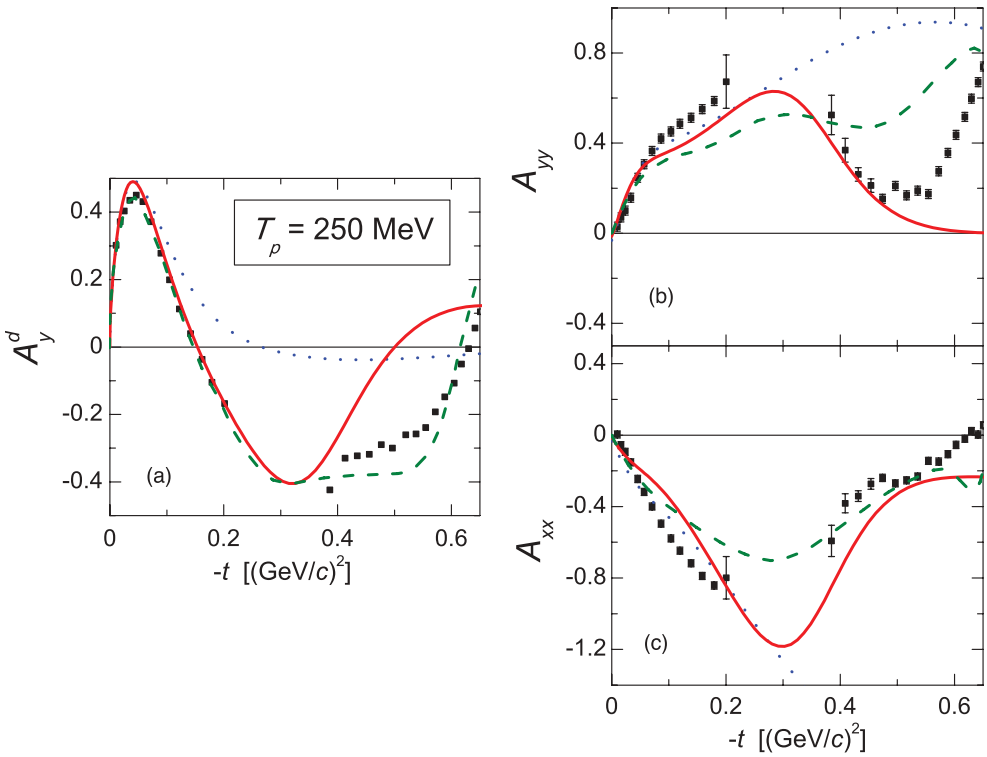

FIG. 3. (Color online) Deuteron vector (a) and tensor (b),(c) analyzing powers in dp elastic scattering at the equivalent proton energy $T_p = 250$ MeV. For the notations, see Fig. 2. Results of the Faddeev calculations and experimental data are taken from Ref. [26] (for the energy $T_p = 200$ MeV).

(b) Or, alternatively, having in our possession the accurate *pd* experimental data in the energy region $T_p > 1.1$ GeV, we can find by inversion the proton-neutron scattering amplitudes which are still poorly known at these energies.

Surely, a separate study should be done before making this inversion to establish here a real sensitivity of the input *pn* amplitudes to the *pd* cross sections and analyzing powers while taking into consideration the experimental error corridor. So, such an inversion opens a way to finding in principle the accurate *nn* (or *pn*) scattering amplitudes from the precise *nd* or *pd* experimental data.

(ii) Our numerous calculations performed in this work on the basis of the refined Glauber model have been compared with the respective exact Faddeev 3*N* calculations with mostly the same input on-shell *NN* amplitudes for differential cross section and vector and tensor analyzing powers. For the numerous spin-dependent observables, it was done for the first time. This direct comparison has demonstrated clearly an amazingly good agreement between the results of the refined diffraction model and exact 3*N* calculations, even at rather low energies, $T_p \simeq 250$ MeV. The agreement gets even more impressive when the collision energy is rising. It should be stressed here that we are observing this nice agreement in the area where the double scattering in the Glauber model approach becomes prevailing. This implies, among other things, that the severe approximations made in the Glauber approach just in the treatment of double scattering [2] really work even at rather low energies.

Our conclusion should be confronted with the results of the previous work [13] where a similar comparison was made between the exact 3*N* Faddeev calculations and the conventional Glauber model predictions for intermediate-energy *Nd* scattering. In that work, both theoretical approaches were based on the simple central *NN* potential MT-III (employed to calculate the input *NN* amplitude for the Glauber model), so the comparison between the predictions was made for differential and total cross sections only. The authors [13] found that in the case of the model *NN* potential MT-III, the Glauber model results do not reproduce the exact 3*N* calculation results for the differential cross section at $T_N \simeq 200$ MeV, and the predictions of both approaches become more similar only at higher energies $T_N \gtrsim 1$ GeV, as should be expected. Nevertheless, a fair agreement between the two approaches was found for the single-scattering terms only, while the Glauber on-shell double-scattering correction was shown to be insufficient in comparison to the Faddeev second-order rescattering correction. Thus, the general conclusion of Ref. [13] was that the Glauber and fully converged Faddeev results *do not coincide* beyond the very forward angles (where the single scattering dominates) even at the highest

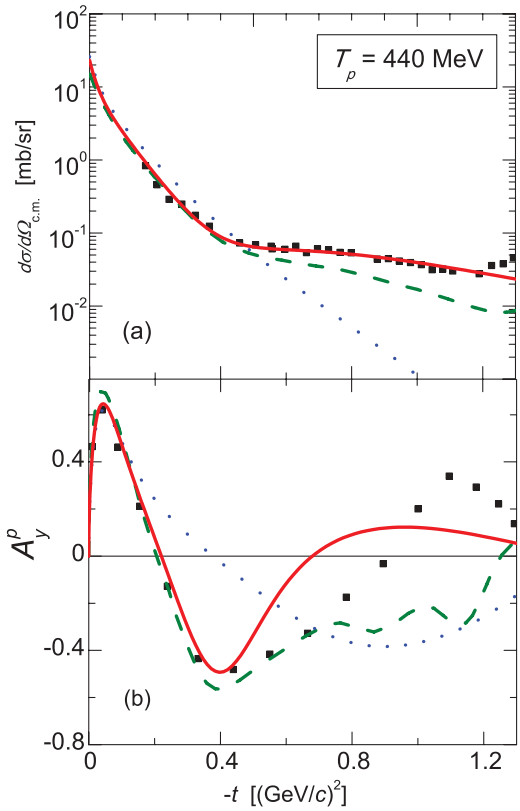

FIG. 4. (Color online) Differential cross section (a) and proton analyzing power (b) in *pd* elastic scattering at the incident energy $T_p = 440$ MeV. For the notations—see Fig. 2. Results of Faddeev calculations are taken from Refs. [11] (440 MeV) and [28] (392 MeV), experimental data—from Refs. [27] (425 MeV) and [28] (392 MeV).

energy considered ($T_N = 2$ GeV). However, when confronting both series of results, one should keep in mind that the model *NN* potential MT-III does not reproduce the empirical *NN* scattering amplitudes at higher partial waves $l \geqslant 1$, and thus does not reproduce the total *NN* amplitudes even at $T_N =$ 250 MeV, see Fig. 6.

It should be stressed that the Glauber approach exploits essentially the characteristic features of just empirical *NN* amplitudes, and that with other types of input *NN* amplitudes, the contributions of neglected terms may become much higher. In particular, the strong sensitivity of the Glauber model results for *pd* scattering (especially in the diffraction minimum) to the ratio of real to imaginary parts of *NN* amplitudes is well known (see, for example, Ref. [31]). Due to numerous inelastic processes at $T_N > 300$ MeV, the realistic *NN* potential has to have an imaginary part rising with energy. This imaginary part of the *NN* potential leads to an *NN* scattering amplitude with enhanced imaginary part, while the amplitude for the model MT-III potential has a very small imaginary part strongly decreasing with the rise of energy (see Fig. 6, upper row).

A second but even more important point is seen from the comparison of the model *NN* differential cross sections (for MT-III potential) with realistic ones (see Fig. 6, lower row). The rates of falling for two types of cross sections (as functions of momentum transfer squared) are completely different, so the effective radius of the *NN* interaction in the realistic case appears to be much shorter than that for the model MT-III interaction. Indeed, the effective radius for MT-III potential $r_{NN} \simeq 2$ fm or even more,[8] so that when analyzing the double-scattering term with such a model input *NN* potential and keeping in mind that the average distance between two nucleons in deuteron is around 4 fm, one can conclude that in this *NN* model the incident nucleon is moving through the target deuteron all the time within a field of strong nuclear force. That is, we cannot consider the incident nucleon in this schematic model as moving freely in between two successive collisions with the nucleons in deuteron. In case of the realistic *NN* interaction, the effective range of the *NN* force gets much shorter as compared to the size of the deuteron (this is clearly seen from Fig. 6), and thus the above assumption of the Glauber model for estimation of the double-scattering term becomes quite valid.

An additional argument in favor of validity of the above Glauber model assumption for the double-scattering term just with the realistic *NN* amplitudes is the good agreement between the diffraction model results and the exact $3N$ calculations found in the present work for many observables, i.e., vector and tensor analyzing powers as well as differential cross sections. In fact, as is seen from Figs. 2–4, the agreement for spin observables is quite evident in the area where the double-scattering term dominates. But this term includes a strong interference between non-spin-flip, single-spin-flip, and double-spin-flip *NN* helicity amplitudes, so that the behavior of the intermediate propagator of the projectile (moving between two successive collisions) should be of high importance in reproducing all the considered spin observables.

(iii) Comparing further the refined Glauber model results with the experimental data and with exact Faddeev results (see Figs. 2–5), one can observe that the area where the diffraction model predictions begin to deviate essentially from the exact $3N$ results almost coincides with that where the latter begin to deviate from experimental data. In other words, the refined Glauber model reproduces quite properly the results of exact $3N$ calculations just in the region where the Faddeev $3N$ framework reflects properly the underlying $3N$ dynamics, i.e., the dynamics which assumes the validity of the conventional $2N$ and $3N$ force models and implies the nucleonic and Δ-isobar degrees of freedom only.

[8] If we define this radius as that value of r_{NN} where the potential can be practically neglected.

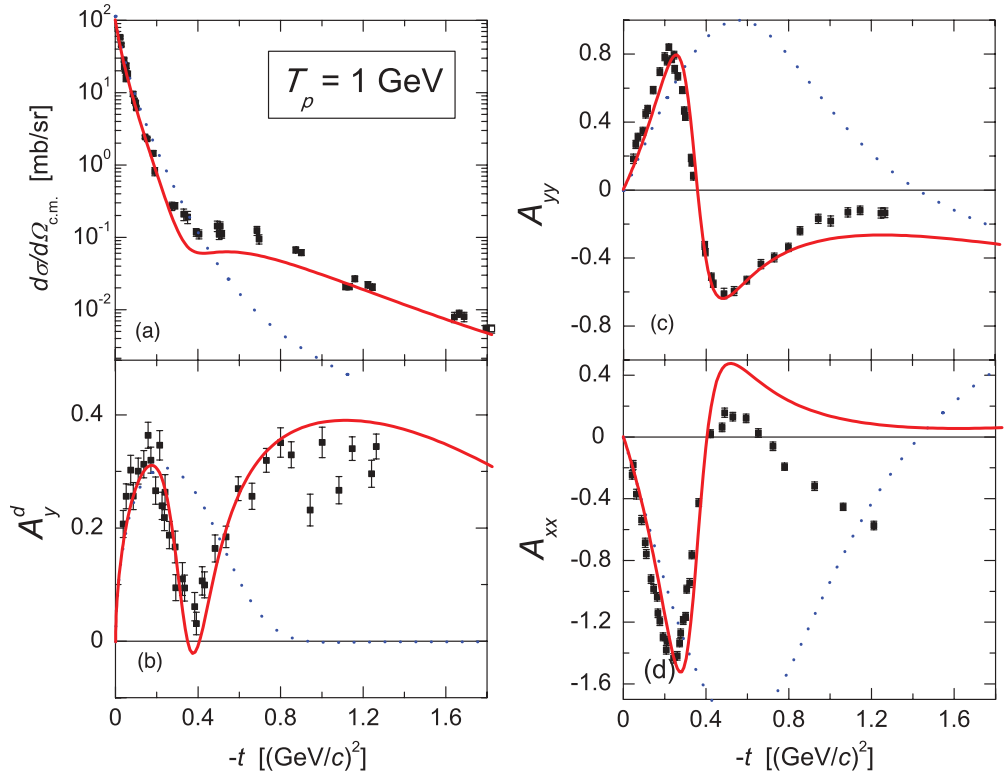

FIG. 5. (Color online) Differential cross section (a) and deuteron vector (b) and tensor (c),(d) analyzing powers in dp elastic scattering at the equivalent proton energy $T_p = 1$ GeV calculated within the refined Glauber model. Dotted lines show the contribution of single scattering only, solid lines represent the full calculation. Experimental data (squares) are taken from Refs. [29,30].

From this point of view, the deviation of the exact Faddeev results from the accurate experimental data on pd scattering [32,33] can imply that some hidden degrees of freedom (e.g., quark-meson) manifest themselves in large-angle pd scattering. A strong additional argument in favor of just this hypothesis follows from the fact that the above deviation gets larger when the collision energy is rising. According to some previous theoretical and experimental works (see, e.g., Refs. [3,34]), the disagreements at 500–1000 MeV may reach an order of magnitude at large scattering angles.

(iv) The last, but not least, problem which can be posed by our Glauber model calculations is related to the amazingly good accuracy of the diffraction model at relatively low energies $T_p \simeq 200$ MeV and at rather large scattering angles. To solve this puzzle, one should recall that when considering scattering of antiprotons by deuteron and other light nuclei, the validity of the Glauber model was found to begin at as low as 50 MeV [35]. The validity of the diffraction model assumptions at such a low energy is undoubtedly related to the strong absorption of antiprotons by the nuclear core, so that the central nuclear area (where the nuclear density is still noticeable) is seen by the incident antiproton as a large black disk, on which the diffraction is observed in such experiments.

Rather similar physics is seen behind the intermediate- and high-energy pd scattering. Because the elastic pd cross section at these energies is a rather small fraction of the total cross section, the dominating processes are just inelastic ones (at least at small and middle impact parameter values), so the fast incident nucleon goes away from the elastic channel with high probability when it is not very far from the loosely bound target nucleus. Thus, the pd elastic scattering at such high energies can be viewed as a diffraction of the fast incident particle on the edge of the large black disk, so the diffraction process can be described as a peripheral collision. This physical picture is schematically represented by Fig. 7. Here the central area (the hatched disk) with the radius $r_t = D_t/2$, with D_t being the size of the deuteron ($D_t \simeq 4$ fm), shows the almost-black disk where the incident nucleons leave the elastic scattering channel and undergo mainly inelastic scattering (an "absorption" from the entrance channel). So, the truly elastic scattering happens mainly at the edge of the hatched disk inside a ring (shown by the dashed line in Fig. 7) with the width λ_i (it corresponds to the wave zone in optical diffraction). Thus, the ratio $\eta_\sigma = \sigma_{\rm el}/\sigma_{\rm tot}$ of the elastic scattering cross section to the total one can be roughly estimated as the ratio of areas inside the ring and hatched inner disk, i.e., $\eta_r = \frac{2\pi r_t \lambda_i}{\pi r_t^2} = 2\lambda_i/r_t$. For the incident energies $T_N \simeq 100$–200 MeV, the

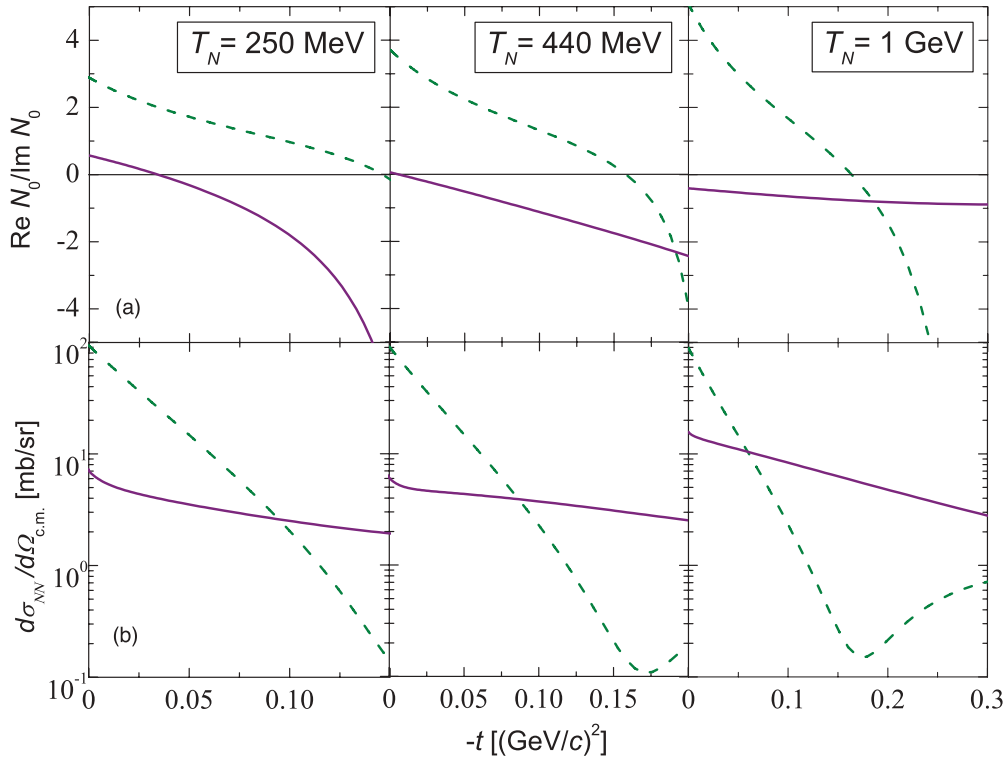

FIG. 6. (Color online) Ratio of the real to imaginary parts of *NN* spin-independent helicity amplitude (a) and *NN* differential cross sections (b) at different energies of the incident nucleon derived from MT-III potential model (dashed lines) and taken from PSA [22] for *np* scattering (solid lines).

nucleon wavelength $\lambda_i \simeq 0.2$–0.3 fm, so the ratio of the areas $\eta_r = 2\lambda_i/r_t \simeq 0.20$–$0.25$, which is in good qualitative agreement with the measured ratio $\eta_\sigma = \sigma_{\rm el}/\sigma_{\rm tot} \simeq 0.15$–$0.20$. From this simple picture, one can understand clearly the reasons for a good applicability of the Glauber diffraction model for the *pd* elastic scattering even at energy $T_p \simeq 200$ MeV.

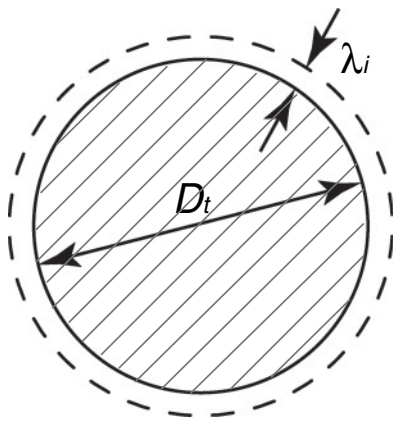

FIG. 7. Illustration of optical diffraction in high-energy *pd* elastic scattering. The almost-black disk with radius $D_t/2$ (hatched disk) surrounded by the wave zone of width λ_i (dashed line) represents the area inside the loosely bound target where inelastic processes dominate. The elastic scattering proceeds mainly in the ring of width λ_i, so that $\lambda_i/D_t \ll 1$.

As for the observed validity of the Glauber model at rather large values of $|t| = q^2$, it is related basically to a double-scattering term which dominates in the region beyond the forward diffraction peak. So, the momentum $\mathbf{q}$ transferred within the double scattering corresponds to ca. $\mathbf{q}/2$ for each of single scatterings entering the double-scattering term. Thus, it is very likely that although the validity of eikonal approximation at $\mathbf{q}/2$ can be broken in a strict sense, the degree of this breaking should increase rather slowly with the rise of q^2.

(v) Finally, it would be very appropriate to discuss here some possible reasons for the observed disagreement between the results of exact $3N$ calculations and experimental data for *pd* cross sections and especially for spin observables at large and backward scattering angles. This topic can be important also in improving the diffraction model description of the experimental data at larger $|t|$ values.

The observation of *pd* differential cross section and spin analyzing powers at large scattering angles shows that starting with incident energy $T_p \simeq 200$ MeV, the disagreements between exact Faddeev calculations and respective experimental data increase when the collision energy rises, and the contribution of conventional $3N$ forces (induced by the intermediate Δ-isobar generation) does not help in reaching the agreement (see the discussion in Ref. [33]). So, it seems that this observation makes it meaningless to

improve the formal aspects of Glauber model by taking into account many other effects ignored in the present formulation, e.g., off-shell corrections and relativistic effects such as boosts, etc., because the majority of these effects have been already included in the exact $3N$ calculations [9] and likely do not help to achieve a good agreement with the data at large angles. It is important to stress also that the experimental differential cross sections at large angles are typically underestimated by the present-day theory. This fact and the rise of all disagreements with energy very likely imply that the theoretical model does not include some essential degrees of freedom which manifest themselves at rising energy stronger and stronger. One can suppose [36] that the most plausible candidature for these d.o.f. ignored in all previous $3N$ calculations are quark-meson (or dressed dibaryon [37,38]) d.o.f. Indeed, the dressed dibaryon describes the situation when two nucleons overlap strongly their quark cores (at $r_{NN} \lesssim 1$ fm). So, according to the modern dibaryon concept [38], this area corresponds to a strong attraction between two quark cores due to an appearance of a strong scalar field surrounding the unified six-quark system. In such a picture, the incident fast nucleon scattered into large angles is feeling not two well-separated nucleons in deuteron but one compact quark bag which can survive, in sharp contrast to loosely bound deuteron, even at very large transferred momenta. Thus, if we assume for a moment the existence of such a quark bag (dressed dibaryon) in deuteron with a weight of about 2–3% [38], it should be sufficient to enhance strongly the backward scattering of intermediate- and high-energy hadrons by deuteron. So, the straightforward generalization of the Glauber model can be done also in this direction.[9]

V. SUMMARY

In this work, we presented the comparison between the predictions for the observables in intermediate-energy *pd* elastic scattering given by the refined Glauber model (with full account of the spin and isospin degrees of freedom), exact Faddeev calculations, and experiments. As input for the refined Glauber model, we used fully realistic *NN* helicity amplitudes which describe the *NN* observables at the intermediate energies (at the level of accuracy of modern PSA) and high-precision model of the deuteron wave function. For the convenient representation of the deuteron radial wave functions and *NN* helicity amplitudes, we employed the special multi-Gaussian expansions which allow us to perform all the calculations fully analytically. So, we calculated within the framework of the refined diffraction model, the *pd* differential cross sections and spin-dependent observables, i.e., the analyzing powers of proton and deuteron, at different energies. We found an amazingly good agreement between the results of our refined Glauber model and exact Faddeev calculations up to transferred momentum values where the exact $3N$ results begin to deviate essentially from the experimental data. We discussed the possible reasons for such surprising agreement, which extends to rather low energy ($T_p \gtrsim 200$ MeV) and rather large scattering angles.

Our general conclusion derived from the detailed comparisons with exact $3N$ calculations and numerous experimental data for *pd* elastic analyzing powers and cross sections can be formulated as follows: the Glauber model (in its refined form developed in the present work) turns out to be quite accurate in a wide angular range starting with relatively low energies for loosely bound target nuclei such as deuteron. The refined diffraction model leads to predictions which are, in general, in a similar agreement with experimental data as the exact Faddeev calculations.

This conclusion should be valid not only for hadron scattering on loosely bound nuclei such as d, ^{6}Li, etc., but also for scattering of such hadrons as η and K and other mesons on arbitrary nuclei, i.e., in the case of strong absorption of an incident wave by the nuclear core.

ACKNOWLEDGMENTS

The authors are very grateful to Prof. A. Faessler for the nice hospitality in Tübingen University where part of this work was done. We appreciate very much the partial financial support from RFBR Grant Nos. 08-02-91959 and 07-02-00609 and the DFG Grant No. 436 RUS 113/790/0-2.

APPENDIX A: INTERRELATIONS BETWEEN *pd* AND *NN* AMPLITUDES IN THE REFINED GLAUBER MODEL

In this Appendix, we present the final formulas of the refined Glauber model. These formulas relate the *pd* invariant amplitudes A_1–A_{12} to the *NN* invariant amplitudes A_i, B_i, C_i, C'_i, G_i, H_i ($i = n, p$) and different components $S_0^{(0)}$, $S_0^{(2)}$, $S_2^{(1)}$, $S_2^{(2)}$ of the deuteron form factor [for the definitions, see Eqs. (3), (8), and (12)]. The general expression for each *pd* invariant amplitude eventually takes the form

$$\begin{aligned} A_j(q) &= \left[A_j^{(s)}(q) + A_j^{(d)}(q) + A_j^{(c)}(q)\right] + [n \leftrightarrow p], \\ A_j^{(d)}(q) &= -\frac{i}{2\pi^{3/2}} \int d^2q' \mathcal{A}_j^{(d)}(\mathbf{q}, \mathbf{q}'), \\ A_j^{(c)}(q) &= -\frac{i}{2\pi^{3/2}} \int d^2q' \left(\mathcal{A}_j^{(d)}(\mathbf{q}, \mathbf{q}') - \mathcal{A}_j^{(c)}(\mathbf{q}, \mathbf{q}')\right), \end{aligned} \tag{A1}$$

where $j = \overline{1, 12}$, and "$+[n \leftrightarrow p]$" denotes an addition of the preceding expression (in square brackets) with the neutron and proton indices interchanged throughout. The formulas for the quantities $A_j^{(s)}$, $\mathcal{A}_j^{(d)}$, and $\mathcal{A}_j^{(c)}$ can be found in Tables I, II, and III, respectively. It is implied there that in single-scattering amplitudes $A_j^{(s)}$, the deuteron form factors are functions of $\mathbf{q}/2$ and invariant *NN* amplitudes are functions of $\mathbf{q}$. In the quantities $\mathcal{A}_j^{(d)}$ and $\mathcal{A}_j^{(c)}$ entering the double-scattering

[9] In doing this, one should consider a direct hadron-dibaryon interaction without basic approximations of the diffraction model such as eikonal, etc.

TABLE I. Formulas for the single-scattering amplitudes $A_j^{(s)}$, $j = \overline{1,12}$ [see Eq. (A1)].

$A_1^{(s)} = (S_0 + \sqrt{2}S_2)A_n$
$A_2^{(s)} = (S_0^{(0)} + \sqrt{2}S_2^{(1)})C_n$
$A_3^{(s)} = -\frac{3}{\sqrt{2}}S_2 A_n$
$A_4^{(s)} = -\frac{3}{\sqrt{2}}S_2^{(1)} C_n$
$A_5^{(s)} = 0$
$A_6^{(s)} = 0$
$A_7^{(s)} = (S_0^{(0)} + \frac{1}{2\sqrt{2}}S_2^{(1)})B_n$
$A_8^{(s)} = 0$
$A_9^{(s)} = (S_0^{(0)} + \frac{1}{2\sqrt{2}}S_2^{(1)})C'_n$
$A_{10}^{(s)} = (S_0^{(0)} + \frac{1}{2\sqrt{2}}S_2^{(1)})(G_n - H_n)$
$A_{11}^{(s)} = (S_0^{(0)} - \frac{1}{\sqrt{2}}S_2^{(1)})(G_n + H_n)$
$A_{12}^{(s)} = 0$

and double-charge-exchange amplitudes ($A_j^{(d)}$ and $A_j^{(c)}$), the deuteron form factors are functions of $\mathbf{q}'$, while in the products of two *NN* amplitudes the first one depends on $\mathbf{q_2}$ and the second one depends on $\mathbf{q_1}$, e.g., $A_n A_p \equiv A_n(\mathbf{q_2})A_p(\mathbf{q_1})$.

In the derivation of $\mathcal{A}_j^{(d)}$ and $\mathcal{A}_j^{(c)}$, we used the following approximate interrelations between the unit vectors:

$$\hat{k} \approx \hat{k}_1 \approx \hat{k}_2, \tag{A2}$$

$$\hat{n}_i\hat{q}_l \approx \hat{q}_i \times \hat{q}_l, \quad \hat{n}_i\hat{n}_l \approx \hat{q}_i\hat{q}_l. \tag{A3}$$

Here $i, l = 0, 1, 2$, and we define $\hat{k}_0 \equiv \hat{k}$, $\hat{q}_0 \equiv \hat{q}$, and $\hat{n}_0 \equiv \hat{n}$ and introduce the unit vectors $\hat{k}_i, \hat{q}_i, \hat{n}_i$ $(i = 1, 2)$ for two individual collisions in the double scattering. The above interrelations are valid within the eikonal approximation.

APPENDIX B: ANALYTICAL CALCULATION OF THE INTEGRALS IN DOUBLE-SCATTERING AMPLITUDES

With the special parametrization of the input *NN* helicity amplitudes and deuteron wave functions presented in Sec. II C, the $\mathbf{q}'$ integration in the double-scattering and double-charge-exchange amplitudes $A_j^{(d)}$ and $A_j^{(c)}$, $j = \overline{1,12}$ [see Eq. (A1)] can be performed fully analytically. In particular, the scalar and vector products of the unit vectors $\hat{q}, \hat{q}', \hat{q}_1, \hat{q}_2$ (appearing in Tables II and III) are expressed through their magnitudes q, q', q_1, q_2 and the angle φ between $\hat{q}$ and $\hat{q}'$ as

$$\begin{aligned}
&\hat{q}\hat{q}' = \cos\varphi, \quad \hat{q}\times\hat{q}' = \sin\varphi,\\
&\hat{q}\hat{q}_1 = (q/2 - q'\cos\varphi)/q_1, \qquad \hat{q}\times\hat{q}_1 = -q'\sin\varphi/q_1,\\
&\hat{q}\hat{q}_2 = (q/2 + q'\cos\varphi)/q_2, \qquad \hat{q}\times\hat{q}_2 = q'\sin\varphi/q_2,\\
&\hat{q}_1\hat{q}' = [-q' + (q/2)\cos\varphi]/q_1, \quad \hat{q}_1\times\hat{q}' = (q/2)\sin\varphi/q_1,\\
&\hat{q}_2\hat{q}' = [q' + (q/2)\cos\varphi]/q_2, \quad \hat{q}_2\times\hat{q}' = (q/2)\sin\varphi/q_2,\\
&\hat{q}_2\hat{q}_1 = \left(q^2/4 - q'^2\right)/(q_2 q_1), \quad \hat{q}_2\times\hat{q}_1 = -qq'\sin\varphi/(q_2 q_1),\\
&q_1^2 = q^2/4 + q'^2 - qq'\cos\varphi, \quad q_2^2 = q^2/4 + q'^2 + qq'\cos\varphi.
\end{aligned} \tag{B1}$$

When multiplying these products by the *NN* amplitudes, the magnitudes q_1 and q_2 in the denominators are exactly canceled with the factors which represent the behavior of the *NN* amplitudes near the origin [see Eq. (15)]. Thus, making use of the expansions for *NN* amplitudes [Eq. (15)] and deuteron form factors [Eq. (17)] and the Eq. (B1), all integrals can be reduced to the standard form

$$\begin{aligned}
J_{nm}(\alpha,\beta;q) &\equiv \int_0^\infty dq' \int_0^{2\pi} d\varphi q'^n e^{-\alpha q'^2 + \beta q q'\cos\varphi}\cos(m\varphi)\\
&= \frac{\pi\Gamma[(n+m+1)/2]\beta^m q^m}{2^m\Gamma(m+1)\alpha^{(n+m+1)/2}}\\
&\quad \times {}_1\mathrm{F}_1((n+m+1)/2, m+1, \beta^2 q^2/(4\alpha)),
\end{aligned} \tag{B2}$$

throughout, where $n \geqslant 1$, $m \geqslant 0$ are integer numbers, and $\alpha = A1 + A2 + 1/(4\lambda)$, $\beta = A1 - A2$ are the combinations of nonlinear Gaussian parameters (λ comes from the deuteron form factors, while $A1$ and $A2$ are related to the *NN* amplitudes depending on $\mathbf{q_1}$ and $\mathbf{q_2}$, respectively). The confluent

TABLE II. Formulas for the quantities $\mathcal{A}_j^{(d)}$ entering the expressions for double-scattering amplitudes $A_j^{(d)}$, $j = \overline{1,12}$ [see Eq. (A1)].

$\mathcal{A}_1^{(d)} = \frac{1}{2}S_0^{(0)}(A_n A_p + 3B_n B_p + (C_n C_p - C'_n C'_p)\hat{q}_2\hat{q}_1 - 2G_n G_p - 2H_n H_p((\hat{q}_2\hat{q}_1)^2 - (\hat{q}_2\times\hat{q}_1)^2)) + \frac{1}{2}(S_0^{(2)} + \sqrt{2}S_2)A_n A_p$
$\mathcal{A}_2^{(d)} = S_0^{(0)}(A_n C_p\hat{q}\hat{q}_1 - C'_n G_p\hat{q}\hat{q}_2 + C'_n H_p((\hat{q}_2\hat{q}_1)(\hat{q}\hat{q}_1) - (\hat{q}_2\times\hat{q}_1)(\hat{q}\times\hat{q}_1))) + \sqrt{2}S_2^{(1)}A_n C_p\hat{q}\hat{q}_1$
$\mathcal{A}_3^{(d)} = S_0^{(0)}(C'_n C'_p(\hat{q}\times\hat{q}_2)(\hat{q}\times\hat{q}_1) - B_n B_p + G_n G_p + H_n H_p((\hat{q}_2\hat{q}_1)^2 - (\hat{q}_2\times\hat{q}_1)^2) + 2G_n H_p((\hat{q}\hat{q}_1)^2 - (\hat{q}\times\hat{q}_1)^2)) - \frac{3}{2\sqrt{2}}S_2 A_n A_p(\hat{q}\hat{q}')^2$
$\mathcal{A}_4^{(d)} = -4S_0^{(0)}C'_n H_p(\hat{q}\times\hat{q}_2)(\hat{q}\times\hat{q}_1)(\hat{q}\hat{q}_1) - \frac{3}{\sqrt{2}}S_2^{(1)}A_n C_p\hat{q}\hat{q}_1(\hat{q}\hat{q}')^2$
$\mathcal{A}_5^{(d)} = S_0^{(0)}(C'_n C'_p(\hat{q}\hat{q}_2)(\hat{q}\hat{q}_1) - B_n B_p + G_n G_p + H_n H_p((\hat{q}_2\hat{q}_1)^2 - (\hat{q}_2\times\hat{q}_1)^2) - 2G_n H_p((\hat{q}\hat{q}_1)^2 - (\hat{q}\times\hat{q}_1)^2)) - \frac{3}{2\sqrt{2}}S_2 A_n A_p(\hat{q}\times\hat{q}')^2$
$\mathcal{A}_6^{(d)} = 2S_0^{(0)}(C'_n G_p - C'_n H_p((\hat{q}\hat{q}_1)^2 - (\hat{q}\times\hat{q}_1)^2))\hat{q}\hat{q}_2 - \frac{3}{\sqrt{2}}S_2^{(1)}A_n C_p\hat{q}\hat{q}_1(\hat{q}\times\hat{q}')^2$
$\mathcal{A}_7^{(d)} = (S_0^{(0)} + \frac{1}{2\sqrt{2}}S_2^{(1)})A_n B_p$
$\mathcal{A}_8^{(d)} = S_0^{(0)}(C'_n G_p\hat{q}\hat{q}_2 + C'_n H_p[\hat{q}\hat{q}_2((\hat{q}\hat{q}_1)^2 - (\hat{q}\times\hat{q}_1)^2) - 2(\hat{q}\times\hat{q}_2)(\hat{q}\times\hat{q}_1)(\hat{q}\hat{q}_1)]) + \frac{3}{\sqrt{2}}S_2^{(1)}A_n C_p(\hat{q}\times\hat{q}_1)(\hat{q}\times\hat{q}')(\hat{q}\hat{q}')$
$\mathcal{A}_9^{(d)} = S_0^{(0)}(A_n C'_p\hat{q}\hat{q}_1 + C_n G_p\hat{q}\hat{q}_2 - C_n H_p((\hat{q}_2\hat{q}_1)(\hat{q}\hat{q}_1) - (\hat{q}_2\times\hat{q}_1)(\hat{q}\times\hat{q}_1))) + \frac{1}{2\sqrt{2}}S_2^{(1)}A_n C'_p(\hat{q}\hat{q}_1 - 3(\hat{q}_1\times\hat{q}')(\hat{q}\times\hat{q}'))$
$\mathcal{A}_{10}^{(d)} = S_0^{(0)}(C_n C'_p(\hat{q}\hat{q}_2)(\hat{q}\hat{q}_1) + A_n G_p - A_n H_p((\hat{q}\hat{q}_1)^2 - (\hat{q}\times\hat{q}_1)^2)) + \frac{1}{2\sqrt{2}}(A_n G_p$ $\times(1 - 3(\hat{q}\times\hat{q}')^2) - A_n H_p[(\hat{q}\hat{q}_1)^2 - (\hat{q}\times\hat{q}_1)^2 - 3(\hat{q}\times\hat{q}')((\hat{q}\hat{q}_1)(\hat{q}_1\times\hat{q}') - (\hat{q}\times\hat{q}_1)(\hat{q}_1\hat{q}'))])$
$\mathcal{A}_{11}^{(d)} = S_0^{(0)}(C_n C'_p(\hat{q}\times\hat{q}_2)(\hat{q}\times\hat{q}_1) + A_n G_p + A_n H_p((\hat{q}\hat{q}_1)^2 - (\hat{q}\times\hat{q}_1)^2)) + \frac{1}{2\sqrt{2}}S_2^{(1)}(A_n G_p(1 - 3(\hat{q}\hat{q}')^2)$ $+ A_n H_p[(\hat{q}\hat{q}_1)^2 - (\hat{q}\times\hat{q}_1)^2 - 3\hat{q}\hat{q}'((\hat{q}\hat{q}_1)(\hat{q}_1\hat{q}') - (\hat{q}\times\hat{q}_1)(\hat{q}_1\times\hat{q}'))])$
$\mathcal{A}_{12}^{(d)} = S_0^{(0)}C'_n B_p\hat{q}\hat{q}_2$

TABLE III. Formulas for the quantities $\mathcal{A}_j^{(c)}$ entering the expressions for double-charge-exchange amplitudes $A_j^{(c)}$, $j = \overline{1, 12}$ [see Eq. (A1)].

$$\mathcal{A}_1^{(c)} = \tfrac{1}{2}S_0^{(0)}(A_nA_n + B_nB_n + (C_nC_n + C_n'C_n')\hat{q}_2\hat{q}_1 + 2G_nG_n + 2H_nH_n((\hat{q}_2\hat{q}_1)^2 - (\hat{q}_2\times\hat{q}_1)^2)) + \tfrac{1}{2}(S_0^{(2)} + \sqrt{2}S_2)A_nA_n$$
$$\mathcal{A}_2^{(c)} = S_0^{(0)}(A_nC_n\hat{q}\hat{q}_1 + C_n'G_n\hat{q}\hat{q}_2 - C_n'H_n((\hat{q}_2\hat{q}_1)(\hat{q}\hat{q}_1) - (\hat{q}_2\times\hat{q}_1)(\hat{q}\times\hat{q}_1))) + \sqrt{2}S_2^{(1)}A_nC_n\hat{q}\hat{q}_1$$
$$\mathcal{A}_3^{(c)} = -\tfrac{3}{2\sqrt{2}}S_2A_nA_n(\hat{q}\hat{q}')^2$$
$$\mathcal{A}_4^{(c)} = -\tfrac{3}{\sqrt{2}}S_2^{(1)}A_nC_n\hat{q}\hat{q}_1(\hat{q}\hat{q}')^2$$
$$\mathcal{A}_5^{(c)} = -\tfrac{3}{2\sqrt{2}}S_2A_nA_n(\hat{q}\times\hat{q}')^2$$
$$\mathcal{A}_6^{(c)} = -\tfrac{3}{\sqrt{2}}S_2^{(1)}A_nC_n\hat{q}\hat{q}_1(\hat{q}\times\hat{q}')^2$$
$$\mathcal{A}_7^{(c)} = S_0^{(0)}(A_nB_n - G_nG_n + H_nH_n((\hat{q}_2\hat{q}_1)^2 - (\hat{q}_2\times\hat{q}_1)^2)) + \tfrac{1}{2\sqrt{2}}S_2^{(1)}A_nB_n$$
$$\mathcal{A}_8^{(c)} = \tfrac{3}{\sqrt{2}}S_2^{(1)}A_nC_n(\hat{q}\times\hat{q}_1)(\hat{q}\times\hat{q}')(\hat{q}\hat{q}')$$
$$\mathcal{A}_9^{(c)} = S_0^{(0)}(A_nC_n'\hat{q}\hat{q}_1 + C_nG_n\hat{q}\hat{q}_2 - C_nH_n((\hat{q}_2\hat{q}_1)(\hat{q}\hat{q}_1) - (\hat{q}_2\times\hat{q}_1)(\hat{q}\times\hat{q}_1))) + \tfrac{1}{2\sqrt{2}}S_2^{(1)}A_nC_n'(\hat{q}\hat{q}_1 - 3(\hat{q}_1\times\hat{q}')(\hat{q}\times\hat{q}'))$$
$$\mathcal{A}_{10}^{(c)} = S_0^{(0)}(C_nC_n'(\hat{q}\hat{q}_2)(\hat{q}\hat{q}_1) + (A_n - B_n)G_n - (A_n + B_n)H_n((\hat{q}\hat{q}_1)^2 - (\hat{q}\times\hat{q}_1)^2))$$
$$+ \tfrac{1}{2\sqrt{2}}S_2^{(1)}(A_nG_n(1 - 3(\hat{q}\times\hat{q}')^2) - A_nH_n[(\hat{q}\hat{q}_1)^2 - (\hat{q}\times\hat{q}_1)^2 - 3(\hat{q}\times\hat{q}')((\hat{q}\hat{q}_1)(\hat{q}_1\times\hat{q}') - (\hat{q}\times\hat{q}_1)(\hat{q}_1\hat{q}'))])$$
$$\mathcal{A}_{11}^{(c)} = S_0^{(0)}(C_nC_n'(\hat{q}\times\hat{q}_2)(\hat{q}\times\hat{q}_1) + (A_n - B_n)G_n + (A_n + B_n)H_n((\hat{q}\hat{q}_1)^2 - (\hat{q}\times\hat{q}_1)^2))$$
$$+ \tfrac{1}{2\sqrt{2}}S_2^{(1)}(A_nG_n(1 - 3(\hat{q}\hat{q}')^2) + A_nH_n[(\hat{q}\hat{q}_1)^2 - (\hat{q}\times\hat{q}_1)^2 - 3\hat{q}\hat{q}'((\hat{q}\hat{q}_1)(\hat{q}_1\hat{q}') - (\hat{q}\times\hat{q}_1)(\hat{q}_1\times\hat{q}'))])$$
$$\mathcal{A}_{12}^{(c)} = 0$$

hypergeometric function ${}_1\mathrm{F}_1$ in our case has positive integer numbers in its first two arguments, so it can be expressed through simple Gaussians and polynomials in q. As a result, one obtains the fully analytical expressions for all *pd* invariant amplitudes A_1–A_{12} in terms of input Gaussian parameters of *NN* helicity amplitudes and deuteron wave functions.

[1] R. J. Glauber, Phys. Rev. **100**, 242 (1955); in *Lectures in Theoretical Physics*, edited by W. E. Brittin *et al.* (Interscience, New York, 1959), Vol. 1, p. 315.
[2] V. Franco and R. J. Glauber, Phys. Rev. **142**, 1195 (1966).
[3] S. A. Gurvitz, Phys. Rev. C **22**, 725 (1980).
[4] J. L. Ballot and L. Lesniak, Phys. Rev. C **38**, 1344 (1988).
[5] G. Alberi, M. Bleszynski, and T. Jaroszewicz, Ann. Phys. (NY) **142**, 299 (1982).
[6] E. Bleszynski, M. Bleszynski, and T. Jaroszewicz, Phys. Rev. Lett. **59**, 423 (1987).
[7] D. R. Harrington, Phys. Rev. **184**, 1745 (1969).
[8] W. Glöckle, H. Witała, D. Hüber, H. Kamada, and J. Golak, Phys. Rep. **274**, 107 (1996).
[9] H. Witała, J. Golak, W. Glöckle, and H. Kamada, Phys. Rev. C **71**, 054001 (2005).
[10] Y. Maeda *et al.*, Phys. Rev. C **76**, 014004 (2007).
[11] K. Suda *et al.*, AIP Conf. Proc. **915**, 920 (2007).
[12] T. Lin, Ch. Elster, W. N. Polyzou, H. Witała, and W. Glöckle, Phys. Rev. C **78**, 024002 (2008).
[13] Ch. Elster, T. Lin, W. Glöckle, and S. Jeschonnek, Phys. Rev. C **78**, 034002 (2008).
[14] E. Kujawski, D. Sachs, and J. S. Trefil, Phys. Rev. Lett. **21**, 583 (1968).
[15] V. Franco, Phys. Rev. Lett. **21**, 1360 (1968).
[16] D. R. Harrington, Phys. Rev. Lett. **21**, 1496 (1968).
[17] V. Franco and R. J. Glauber, Phys. Rev. Lett. **22**, 370 (1969).
[18] C. Wilkin, Phys. Rev. Lett. **17**, 561 (1966).
[19] R. J. Glauber and V. Franco, Phys. Rev. **156**, 1685 (1967).
[20] M. N. Platonova and V. I. Kukulin, Yad. Fiz. **73**, 90 (2010) [Phys. At. Nucl. **73**, 86 (2010)]; M. N. Platonova, Preprint No. 2009-2/846, SINP MSU, 2009 (unpublished).
[21] C. Sorensen, Phys. Rev. D **19**, 1444 (1979).
[22] R. A. Arndt, W. J. Briscoe, I. I. Strakovsky, and R. L. Workman, Phys. Rev. C **76**, 025209 (2007); the full SAID database can be accessed at http://gwdac.phys.gwu.edu.
[23] M. Matsuda, J. Nagata, H. Yoshino, and Y. Yoshino, Comput. Phys. Commun. **131**, 225 (2000).
[24] R. Machleidt, Phys. Rev. C **63**, 024001 (2001).
[25] K. Hatanaka *et al.*, Phys. Rev. C **66**, 044002 (2002).
[26] B. v. Przewoski *et al.*, Phys. Rev. C **74**, 064003 (2006).
[27] N. E. Booth *et al.*, Phys. Rev. D **4**, 1261 (1971).
[28] A. Tamii *et al.*, Mod. Phys. Lett. A **18**, 440 (2003); AIP Conf. Proc. **915**, 765 (2007).
[29] G. W. Bennett *et al.*, Phys. Rev. Lett. **19**, 387 (1967).
[30] M. Haji-Saied *et al.*, Phys. Rev. C **36**, 2010 (1987).
[31] V. Franco and E. Coleman, Phys. Rev. Lett. **17**, 827 (1966).
[32] K. Sekiguchi, Nucl. Phys. **A805**, 250 (2008), and references therein.
[33] K. Sekiguchi, Eur. Phys. J. (to be published).
[34] J. S. Vincent *et al.*, Phys. Rev. Lett. **24**, 236 (1970).
[35] Yu. N. Uzikov and J. Haidenbauer, Phys. Rev. C **79**, 024617 (2009), and references therein.
[36] V. I. Kukulin and M. N. Platonova, Eur. Phys. J. (to be published).
[37] A. Faessler, V. I. Kukulin, and M. A. Shikhalev, Ann. Phys. (NY) **320**, 71 (2005).
[38] V. I. Kukulin, I. T. Obukhovsky, V. N. Pomerantsev, and A. Faessler, Int. J. Mod. Phys. E **11**, 1 (2002); V. N. Pomerantsev, V. I. Kukulin, V. T. Voronchev, and A. Faessler, Yad. Fiz. **68**, 1511 (2005) [Phys. At. Nucl. **68**, 1453 (2005)].